Vibratory Behavior of Twisted Cantilevered Plates

James C. MacBain*
Air Force Aero Propulsion Laboratory, Wright-Patterson Air Force Base, Ohio

A combined numerical-experimental study of the effects of varying tip twist and increasing centrifugal loading on the resonant characteristics of cantilevered plates is presented. The finite element computer program, NASTRAN, is used to compute the natural frequencies, mode shapes, and normalized shear stress distribution for each mode of vibration for cantilevered plates having, a), varying degrees of tip twist and, b) increasing centrifugal loading. For the case of zero centrifugal load, the resulting mode shapes are compared to those obtained experimentally using holographic interferometry. The agreement between the two is found to be quite good. For increasing centrifugal loading, it is found that the nodal lines of the flexural modes of vibration shift toward the plate root. Increased centrifugal loading is also found to strongly effect the character of some of the plate-like vibration modes of the cantilevered plate.

Nomenclature

E = Young's modulus, lb/in.^{2}
L = plate length, in.
$(N\text{x}M)$ = finite element mesh composed of N grid points across plate width and M grid points along plate length
nF = nth flexural mode of vibration
nT = nth torsional mode of vibration
PM_n = nth plate mode of vibration
R = disk radius, in.
t = plate thickness, in.
w = plate width, in.
x = axial distance along plate
y = chordwise distance along plate
z = distance normal to plate
θ_T = angle cantilever free end makes with y axis, deg.
λ = nondimensional frequency
ν = Poisson's ratio
ρ = mass density, lbm/in.^{3}
Ω = angular velocity of disk supporting twisted plate, rpm
ω = circular frequency, rad/sec

Introduction

KNOWLEDGE of the resonant characteristics of turbine and compressor blades is of utmost importance in insuring reliable long-life turbine engines. The damage caused by blades failing due to vibratory fatigue can be catastrophic at worst and at the very least result in additional engine development costs due to redesign and repair. Comprehensive analytical and experimental methods for analyzing the vibrational characteristics of turbine blading are essential in the avoidance and prediction of turbine engine blade vibration problems.

Much of the early work carried out in studying the vibration characteristics of turbine blading was based on the assumptions of simple beam theory. Rosard,[1] Carnegie,[2] Isakson and Eisley,[3] and Houbolt and Brooks,[4] among others, used simple beam theory and various solution techniques to study the vibratory behavior of twisted cantilever beams as an analog for twisted propellers and turbine blading. While these works were complete in their own right, their techniques could not adequately handle the newer lightweight, low aspect ratio turbine blading where the blades are more likely to behave as plates or shells rather than beams. The solution to this dilemma arrived with the advent of finite element analysis methods. Now, a blade having a complex geometry can be accurately modeled as a composition of many elastic elements having well-defined elastic properties. Anderson, Irons, and Zienkiewicz[5] aptly demonstrated the utility of finite element analysis in studying the vibration and stability behavior of thin plates for various geometries and boundary conditions. Rawtani and Dokainish[6,7] have very effectively used finite element techniques to study the vibration behavior of twisted cantilever plates. They analyzed the effect of varying degrees of pretwist on the natural modes and frequencies of cantilevered plates.[6] They also carried out a vibration analysis of a flat cantilevered plate fixed to a rotating disk.[7] The effects of plate inclination, disk radius, and angular velocity on the plate's natural frequencies and mode shapes were studied.

The work described serves the valuable function of raising additional questions, some of which the present paper addresses. In the present analysis the normalized stress distribution corresponding to each of the natural mode shapes of a twisted cantilevered plate is studied. The natural modes, frequencies and maximum shear stress distribution are computed for cantilevered plates having varying degrees of tip twist using the general purpose finite element computer program, NASTRAN. The resulting mode shapes are compared to those obtained experimentally using holographic interferometry. The effect of centrifugal loading or the vibratory response of a twisted cantilevered plate is also studied.

Finite Element Model of Twisted Plate

The numerical portion of the study was based on a finite element model of a twisted cantilever plate. The geometry of the model is shown in Fig. 1. Using this model

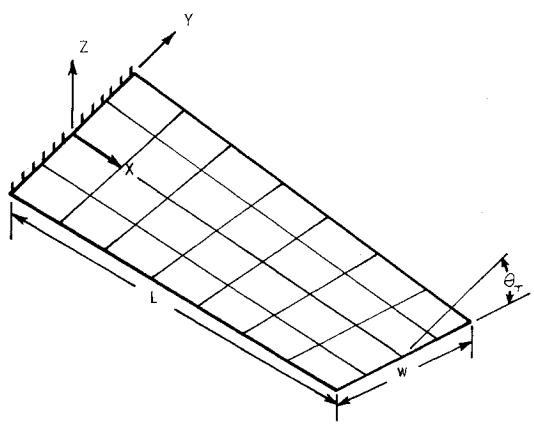

Fig. 1 Cantilever plate: finite element model (N = 5, M = 8).

Received July 29, 1974; revision received October 25, 1974.
Index categories: Structural Dynamic Analysis; Computer Technology and Computer Simulation Techniques; Lasers.

*Member of Structural Integration and Analysis Group, Propulsion Branch, Turbine Engine Division.

the multipurpose finite element computer program NASTRAN (level 15.1.1) was used to compute the natural frequencies and mode shapes for cantilever plates having a) increasing values of the tip twist Θ_T and b) for increasing centrifugal loading with $\Theta_T = 30°$.

The base of the model cantilever plate was fixed against translation and rotation. The plate had a linearly varying twist about the x-axis resulting in a maximum twist of Θ_T at the free end. For this geometry, the grid point coordinates for a plate having a tip twist Θ_T are given by:

$$x = (K-1)/(M-1)L \tag{1}$$

$$y = [(J-1)/(N-1) - 1/2]w \cos(x\Theta_T/L) \tag{2}$$

$$z = [(J-1)/(N-1) - 1/2]w \sin(x\Theta_T/L) \tag{3}$$

$$J = 1, 2 \ldots N$$

$$K = 1, 2 \ldots M$$

where L and w are the length and width of the plate, respectively, and N and M are the number of grid points along the plate width and length, respectively. It should be noted that in using Eqs. (1-3) to generate the mesh, it is tacitly assumed that the plate length, L, remains constant across the beam width. In reality, the maximum value of the "x" coordinate would become increasingly smaller than the length for increasing tip twist, Θ_T. For example, for $\Theta_T = -30°$ and $w = 3$, the present geometric assumptions make the length along the plate edge take on a value of 1.005 L. Using Eqs. (1-3), a finite element mesh made up of quadrilateral elements was generated that described the twisted plate.

The type of element used was the quadrilateral plate bending element (CQUAD2) familiar to NASTRAN users.[8] The quadrilateral element was chosen over the available triangular elements (CTRIA2) because the former element gave smoother, more continuous, stress contour plots than the latter for a given set of grid points. This phenomenon is most probably because NASTRAN computes stresses at each element's centroid and in a mesh composed of triangular element, each element's centroidal location is not symmetrical with respect to its neighboring elements' centroids. In the case of a quadrilateral mesh, symmetry exists between adjacent elements' centroids. The fact that quadrilateral elements do not allow strict adherence to a doubly curved surface has no appreciable effect on the results provided that the actual surface curvature per element is small. Such was the case in this analysis.

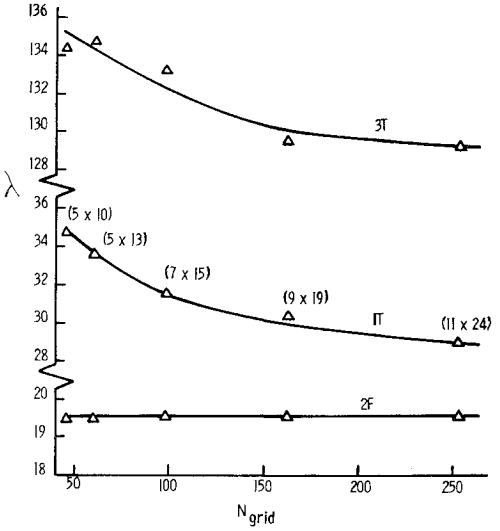

Fig. 2 Natural frequency vs number of grid points ($\Theta_T = -30°$).

To determine the proper size of the mesh for sufficiently accurate modes and frequencies, test cases were run for a cantilever plate having a $-30°$ tip twist ($\Theta_T = -30°$) and meshes of increasing size. A mesh will be said to be ($N \times M$) if it has N grid points across its width and M grid points along its length. This, of course, yields a total of $N \cdot M$ grid points. For this test and all those to follow in this analysis, the cantilever plate was assumed to have the following properties: length, $L = 7$ in., width, $w = 3$ in., thickness, $t = 0.090$ in., Young's modulus, $E = 1 \times 10^7$ psi, Poisson's ratio, $\nu = 0.3$, and mass density, $\rho = 2.587 \times 10^{-4}$ lbm/in.^{3}

Using these properties and the specified value of Θ_T, the eigenvalue extraction routine in NASTRAN[8] (rigid format 3-inverse power method) was used to determine the natural frequencies of the twisted plate for varying mesh size. Figure 2 shows how the natural frequency converges for increasing mesh size for the vibration modes, second bending (2F), first torsion (1T), and third torsion (3T). The frequency is plotted in terms of a nondimensional frequency parameter λ vs the total number of unfixed grid points for each mesh where

$$\lambda = \omega\left(\frac{\rho t L^4}{D}\right)^{1/2}$$

$$D = Et^3/12(1-\nu^2) \tag{4}$$

Also shown in the figure, along the first torsion convergence curve (1T), is the mesh order ($N \times M$) for each test point. It is seen that the second bending curve is essentially flat indicating convergence to a constant value of the frequency for some value of N_{grid} less than 45. This type of rapid convergence was characteristic of all the bending modes of vibration in this study. In contrast, the torsional modes converged more slowly as evidenced by the curves for first and third torsion in Fig. 2. This slower rate of convergence is apparently caused by the twisted geometry of the plate, since in the case of a flat plate ($\Theta_T = 0$), convergence rates for both bending and torsional modes were the same. Finally, we note from Fig. 2 that for all of the modes, convergence has been achieved for mesh order ($N \times M$) = (11×24). This mesh size was used in the following study.

As a check on the accuracy of using the (11×24) mesh size, Table 1 shows a comparison of the first four natural frequencies for a flat plate with the results obtained by Barton[9] using the Rayleigh-Ritz energy method. It is seen that the two sets of results agree well, the worst case being a difference of -2.4% for the second torsional mode.

Results of Finite Element Vibration Analysis (*rpm* = O)

The natural frequencies, mode shapes, and maximum shear stress distribution for each normalized mode were determined for finite element models of the twisted cantilevered plate having tip twist values of $\Theta_T = 0°$, $-12°$, $-17°$, $-23.5°$, $-30°$, and $-38°$. These values of the tip twist angle were chosen to match those of actual cantilevered twisted plates whose modes and frequencies were experimentally determined. The experimental results will be discussed in a later section. The values of Θ_T are nega-

Table 1 Nondimensional frequencies of a flat cantilevered plate ($\nu = .3$, $L/w = 2.33$)

Mode	NASTRAN	Barton[9]	% Difference
1F	3.43	3.47	−1.2
1T	16.74	17.10	−2.1
2F	21.36	21.58	−1.0
2T	53.66	55.00	−2.4

Table 2 Natural frequency as a function of tip twist

	Tip twist, Θ_T (deg)											
	0		−12		−17		−23.5		−30		−38	
Mode	F.E.	Exp.	F.E.	Exp.	F.E.	Exp.	F.E.	Exp.	F.E.	Exp.	F.E.	Exp.
1) $1F$	3.429	3.45	3.436	3.22	3.443	3.22	3.456	3.16	3.473	3.39	3.501	3.22
2) $1T$	16.74	16.79	19.44	17.42	21.74	19.89	25.22	23.06	28.99	27.54	33.71	30.93
3) $2F$	21.36	21.50	21.03	19.43	20.71	18.86	20.18	18.17	19.56	19.09	18.75	16.79
4) $2T$	53.66	53.76	59.44	53.82	64.61	59.28	72.85	66.29	82.08	76.87	93.99	82.68
5) $3F$	59.94	60.37	59.36	56.12	58.86	55.02	58.14	53.87	57.38	57.84	56.50	55.71
6) PM_1	81.01	...	82.48	...	83.87	73.71	86.09	86.47	88.74	100.21	93.36	104.35
7) $3T$	100.3	100.8	105.6	101.5	110.7	102.6	119.2	109.5	129.3	123.6	143.2	130.8
8) $4F$	115.4	117.2	115.6	111.1	115.8	111.0	116.0	108.7	116.1	115.0	116.4	108.1
9) PM_2	124.2	131.8	125.3	131.7	126.4	133.4	128.3	134.8	130.8	136.4	134.7	143.2
10) PM_3	153.6	161.2	155.9	160.2	158.2	161.1	162.2	162.5	167.4	168.4	175.4	171.0
11) $4T$	161.3	...	165.1	...	168.9	...	...	...	...	...	...	...

tive in the sense of the right-hand rule along the x-axis of the coordinate system in Fig. 1. For all computer runs of NASTRAN, the $(N \times M) = (11 \times 24)$ finite element model was used in the analysis.

The resulting natural frequencies are shown in Table 2 in nondimensional form for the different values of Θ_T in the columns giving values based on finite element analysis (F.E.). The type of mode of vibration is also given for each case where F corresponds to flexure or bending, T corresponds to torsion, and PM indicates a plate mode, i.e., a mode that would not result from a vibration analysis based on simple beam theory. Three such plates modes were found in the frequency range of interest in this study. One of these (PM_1) has some rather interesting characteristics which will be discussed later.

The frequencies based on finite element analysis in Table 2 are shown plotted as a function of tip twist in Figs. 3 and 4. The trends shown in these two figures exhibit characteristics which are typical of how plate frequencies vary with increasing twist.[2,6] The first mode, $1F$, is practically insensitive to increasing Θ_T and increases by only 2% as Θ_T goes from 0 to 38°. The higher flexural modes are also relatively insensitive to increasing values of Θ_T. In contrast, the torsional modes are very sensitive to the tip twist and exhibit a marked increase in value as Θ_T increases. For example, comparing modes 2F and $1T$ in Fig. 3, as Θ_T increases from −0° to −38°, mode $2F$ decreases in value by 12% while made $1T$ shows a 100% increase. The three plate modes shown in the figures also increase with increasing Θ_T, though not quite as strongly as the purely torsional modes of vibration.

In addition to computing natural frequencies, the version of NASTRAN used at the Air Force Aero Propulsion Laboratory permits contour plots to be made of the vibration mode shapes as well as the stresses based on the normalized modal deflection. This version of NASTRAN is known as level 15.1.1. The addition of contour plotting to the structural plotting module in NASTRAN was carried out at the Naval Ship Research and Development Center.[10]

For the plate having a tip twist of −30°, contour plots of the displacement in the z-direction (normal to the plane of the plate) and of the maximum shear stress distribution were generated for the first ten modes of vibration. Figures 5 and 6 show the contour plots of the z-displacement for the first ten modes of the −30° plate. The plate is positioned in the figures such that the z-axis (Fig. 1) is into the page. The fixed end of the plate is at the bottom of the figure. The contour numbers in the figures correspond to values of the displacement in the z-direction such that the integers 1, 2, 3, 4, 5, 6, 7, 8, 9, 10, 11 refer to the z-displacement values −1., −0.8, −0.6, −0.4, −0.2, 0,

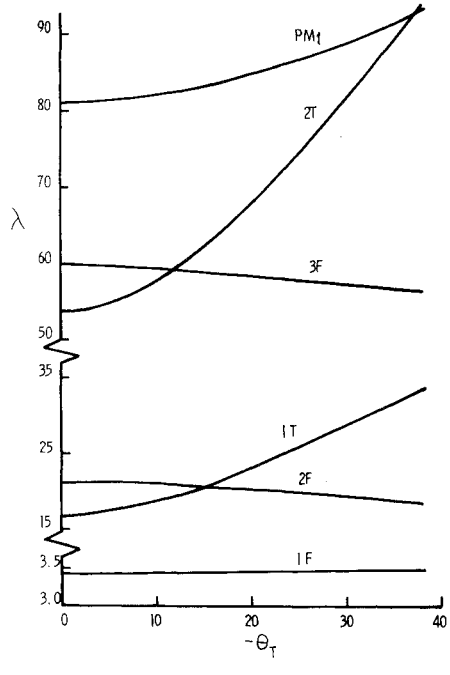

Fig. 3 Natural frequency as a function of tip twist (Modes 1-6).

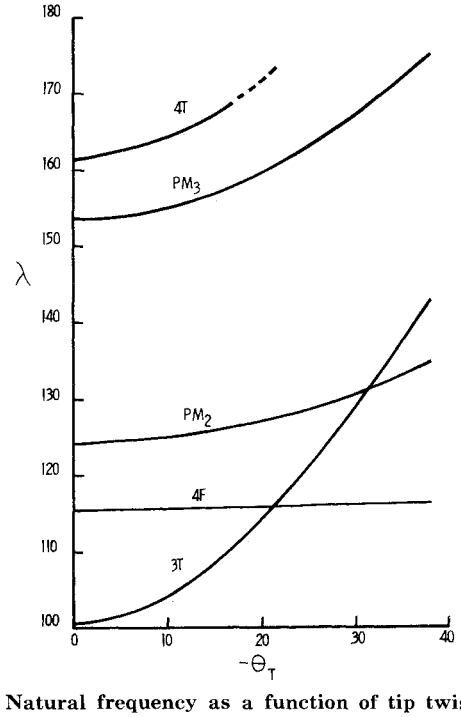

Fig. 4 Natural frequency as a function of tip twist (Modes 7-11).

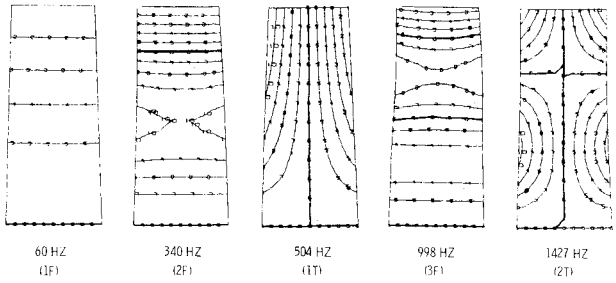

Fig. 5 Mode shapes 1-5 of cantilevered plate ($\Theta_T = -30°$).

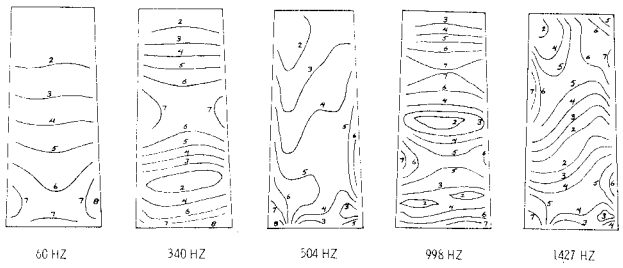

Fig. 7 Maximum shear stress distribution of mode shapes in Fig. 5.

0.2, 0.4, 0.6, 0.8, 1., respectively. Note that contour number 6 corresponds to a z-displacement of zero and hence, defines the vibration nodal lines for each mode shape. For the purposes of this paper, the nodal lines were further darkened by hand to enhance their visibility.

The contour plots serve to graphically display the deformation characteristics of each mode of vibration. Note that all of the modes exhibit either a symmetrical displacement about the long plate axis (x-axis). All but one of the modes are typical of classical plate vibration response. There are the commonly observed flexural and torsional modes, PM_2 is the "Lyre mode" at 2275 Hz, and PM_3 is another classical plate mode at 2912 Hz. The plate mode at 1543 Hz (PM_1 in Fig. 3) is rather unusual in that it has a nodal line at about the two-third span similar to a second bending ($2F$) mode but below this deforms into a saddle shape indicating chordwise bending. The nodal line at the plate base, extending outward like a peninsula is particularly unique.

An intuitive guess backed up by some experimental observations of the PM_1 mode suggests that the mode is a result of the coupled vibration of two other distinct vibratory modes, the coupling being caused by the plate's twisted geometry. This premise was supported by the experimental tests where the PM_1 was visually observed using holographic interferometry. As plates with decreasing values of Θ_T were tested, the PM_1 mode became more and more difficult to find. For the values of $\Theta_T = 0°$ and $-12°$, it did not show up at all experimentally.

While Figs. 5 and 6 show the first ten mode shapes only for the plate having $\Theta_T = -30°$, the mode shapes for the plates for the other values of tip twist followed the same patterns shown in the figures but occurred at different frequencies as previously discussed.

In addition to the mode shapes, contour plots of the normalized maximum shear stresses were also computed for the first ten vibration modes of the cantilevered plate having a $-30°$ tip twist. The maximum shear stress contours were output in the same computer runs of NASTRAN as the mode shapes and are "normalized" in the sense that their value for each mode shape is based upon a maximum modal z-displacement of unity. As in the case of the displacement contours, each maximum shear stress contour is assigned an integer which corresponds to a given value of the maximum shear stress in the NASTRAN printout. In this analysis the range of maximum shear stress was divided into eight equal increments for each vibration mode. Thus, in the contour plots shown in Figs. 7 and 8, the contour numbers ranging from 1 to 8 correspond to increasingly greater values of the maximum shear stress. Since the value of the maximum shear stress is based on the normalized mode shape, its magnitude has no significance. It is the trends demonstrated by the contour plots (areas of greatest maximum shear stress) that are important.

Some observations with regard to the maximum shear stress distribution are in order. Looking at Figs. 7 and 8 we see that the twisted plate geometry has a significant effect on the shear stress distribution for the torsional modes (mode 1T at 504 Hz, for example) but not as great an effect for the flexural modes, the flexural modes being relatively symmetrical about the plates twist axis (x-axis). For the case of a flat plate ($\Theta_T = 0$, not shown) the maximum shear stress contours were found to be symmetrical about the twist axis for both flexural and torsional modes of vibration. Finally, it should be noted that since we are seeing stress contours while the plate is at one of its extreme positions, a mirror image of the stress distribution will result when each mode reverses itself by a phase angle of 180°.

It is also evident from Figs. 7 and 8 that anticlastic bending of the plate along its sides contributes to an increase in the maximum shear stress. An example of this is seen for the case of the first bending mode (60Hz) at the plates edge near the fixed end and also for the case of the second bending mode (340 Hz) at the plate's edge around the midspan location. The last three modes in Fig. 8 are of particular interest in that they all have an area of greatest maximum shear stress at their tips, a condition to be avoided in turbine blading.

In general, Figs. 7 and 8 give some insight into the maximum shear stress distribution of each of the mode shapes shown in Figs. 5 and 6. This type of information is particularly helpful when one has to predict highly stressed areas based on modal vibration data from (say) holography tests or scattered localized strain gage data.

Plate Vibration Behavior under Centrifugal Loading

The analysis in the preceding section proved informative as to the vibration behavior and modal stress distri-

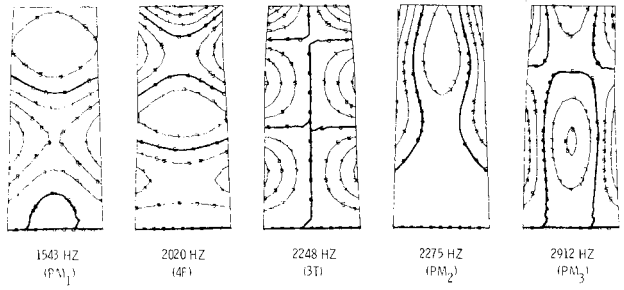

Fig. 6 Mode shapes 6-10 of cantilevered plate ($\Theta_T = -30°$).

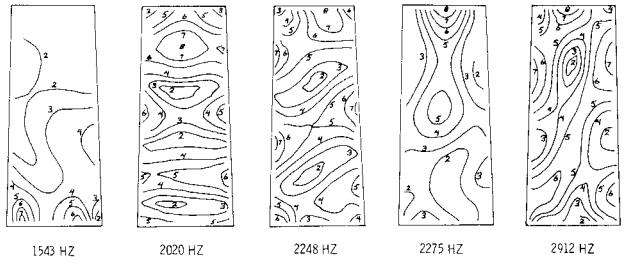

Fig. 8 Maximum shear stress distribution of mode shapes in Fig. 6.

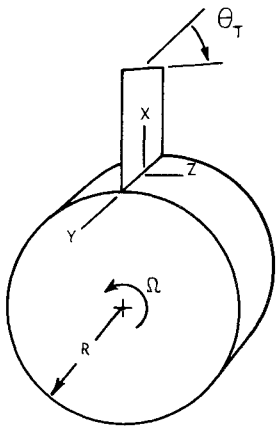

Fig. 9 Twisted plate attached to rotating disk.

bution of twisted cantilever plates. In keeping with using the twisted plate as an analog for turbine blading, it is instructive to study its vibratory response under the additional influence of centrifugal loading. How are the mode shapes and natural frequencies affected by centrifugal loading caused by an induced RPM? To study this, the cantilevered plate having a −30° tip twist was assumed to be fixed to a disk of radius R, rotating at some angular velocity as shown in Fig. 9. For the present analysis, the disk radius was held fixed at $R = 7''$.

Rigid format 13 of NASTRAN was used to compute the first six natural frequencies and mode shapes of the −30° plate for specified values of the angular velocity, Ω. NASTRAN accomplishes the vibration analysis in a two-step operation. First, it takes the value of the angular velocity input to it and creates a set of forces that act on the element centroids of the finite element model. These forces are of course a function of the elements' masses, their location with respect to the axis of rotation, and the angular velocity. Using these forces, a static analysis is carried out (rigid format 1) and the resulting stresses are used to generate a centrifugal stiffness matrix. In the second step of the operation, the centrifugal stiffness matrix is added to the NASTRAN generated elastic stiffness matrix and an eigenvalue analysis is carried out (rigid format 3) yielding the natural frequencies and mode shapes of the structure. This two-step process is carried out automatically using rigid format 13 of NASTRAN.

The first six natural modes and frequencies of the −30° plate were computed as a function of the disk angular velocity Ω where Ω ranged from 0 to 18,000 RPM. Figure 10 shows the first six natural frequencies as a function of RPM. As one might expect, the flexural modes are more strongly effected by increasing RPM than the torsional modes. The first plate mode (PM_1) closely parallels the second torsional mode ($2T$). This would seem to support the premise that the second torsional mode is one of the contributing components in the coupled bending-torsional nature of mode PM_1. The dashed lines in the curves for modes PM_1 and $2T$ indicate an extrapolation of these curves past Ω = 12,000 rpm.

Along with computing the natural frequencies as a function of Ω, the natural mode shapes were also computed. The first six mode shapes corresponding to an angular velocity of Ω = 12,000 rpm in Fig. 10 are shown in Fig. 11. As in the preceding contour plots of mode shapes, contour number 6 (thick lines) represents the zero z-displacement contour or nodal line. Some close scrutiny of Fig. 11 brings out some interesting points. For the purely flexural modes and torsional modes above first torsion, the effect of centrifugal loading on the vibration mode shape is to translate the modal lines running in the chordwise direction toward the plate root. In addition, increased anticlastic behavior of the plate is apparent as evidenced by a slight increase in the curvature of the chordwise nodal lines. An example of this can be seen by comparing mode $3F$ in Fig. 11 with mode $3F$ in Fig. 5 where Ω = 0. The trends demonstrated here with regard to nodal line shift are similar to the findings of Henry[11] in his study of rotating compressor blades.

The last mode ($3F'$) shown in Fig. 11 is particularly interesting. This is actually mode PM_1 (see Fig. 6) but the centrifugal loading has caused a nodal line shift such that three chordwise nodal lines now exist instead of two as was the case for Ω = 0. The mode is denoted as "$3F'$" in Fig. 11 since it now has the appearance of the third flexural mode ($3F$). The result raises the interesting question of whether there are other plate geometries (length to width ratio, twist, etc.) such that a given centrifugal loading would cause other "multiple" modes to occur.

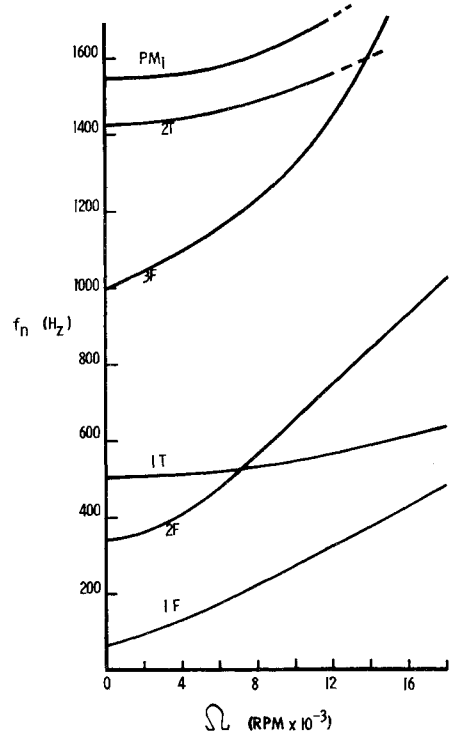

Fig. 10 Natural frequency as a function of angular velocity ($\Theta_T = -30°$).

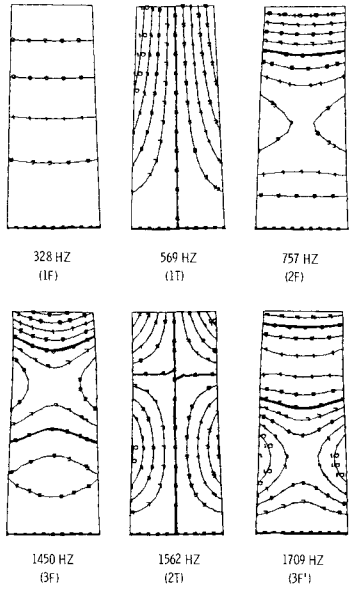

Fig. 11 Mode shapes of cantilevered plate ($\Theta_T = -30°$, Ω = 12,000 rpm).

Experimental Vibration Tests of Twisted Plate

The results of the finite element analysis of a twisted plate having varying degrees of tip twist were experimentally checked by means of holographic interferometry at the AFAPL's Turbo-Structures Research Laboratory (TSRL). The application of holographic interferometry to vibrating objects is an ideal method of experimentally determining the object's natural modes and frequencies of vibration. It was first used to study vibrating objects by Powell and Stetson[12,13] in 1965 and has since proved particularly useful for vibration analysis in that the object under study is not contacted, can be any shape, and the final result consists of a full field picture of the vibrating object's displacement.

A hologram is made when a high resolution photographic plate is exposed to two beams of coherent light waves intersecting at the photographic plate's surface. The fact that the light waves are spatially and temporally coherent (in step with each other in space and time) enables a grating to be formed on the plate. This grating is formed from the constructive and destructive interference of the two light beams. After the plate has been developed, returned to its original position, and illuminated by one of the original light beams, the grating on the plate will cause the light to be bent or diffracted such that the second light beam is recreated. If this second light beam is composed of the light waves diffusely reflected off an object, the image of the object is reconstructed. Furthermore, it appears in its original position if all other factors are the same as in the original exposure. It is this unique property that is the basis for holographic interferometry.

In using the technique for vibration analysis, a hologram is made of the object to be analyzed (a plate in this case) while it is stationary. When the hologram is developed and placed in its original position, one observes a superposition of the original object and the image of the object reconstructed by the hologram. If the object is vibrated or displaced, fringes will be seen to appear. The fringes are caused by the light rays from the object interfering with those from the image and correspond to the displacement of the object from its original stationary position. If the object is excited sinusoidally, fringes will be seen on the object only when all points on the object are vibrating in phase or 180° out of phase with each other. Such is the case when an elastic body is vibrating at one of its natural frequencies. Thus, by sweeping through the frequency range of interest, the natural frequencies and mode shapes can be determined by observing at what frequencies the fringes occur and how they are distributed. This type of testing is termed "real-time" holography in that the fringes appear or disappear as a result of actually occurring stimuli.

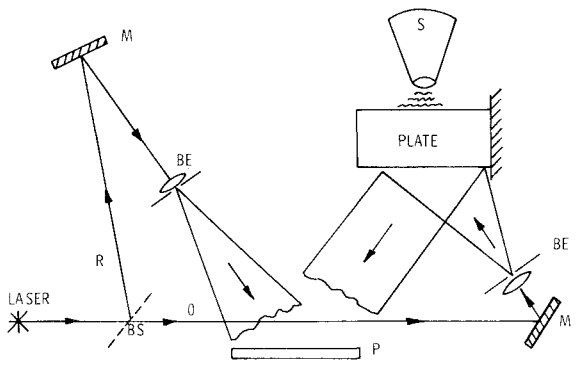

Fig. 12 Schematic of experimental set-up: BS-beam splitter, M-mirror, BE-beam expander, P-photographic plate, S-siren.

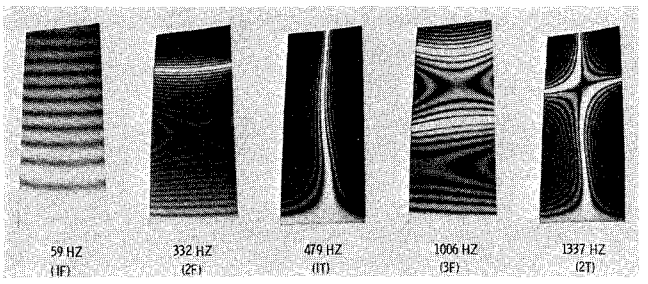

Fig. 13 Experimental mode shapes 1–5 of cantilevered plate ($\Theta_T = -30°$).

Once the natural frequencies for the object have been determined using "real-time" holography, permanent records of the natural mode shapes are made using "time-average" holography. This method consists of exposing the photographic plate while the object is vibrating at one of its natural frequencies. The resulting hologram shows the object to be covered with interference fringes. Basically, these fringes are caused by interference when the object is at its two extreme oscillatory locations. The points on the object that do not move, i.e, the nodal lines, reflect the most light and appear as the brightest fringes in the hologram. Traveling outward from the nodal lines each fringe encountered represents a contour of constant displacement. Hence, the time-average hologram yields a contour map of the object's normal displacement. For a more in-depth treatment of holographic interferometry, the reader is referred to the text by Collier,[14] et al.

The experimental setup used to determine the natural modes and frequencies of the twisted plates is shown schematically in Fig. 12. A HeNe 50 MW laser (Spectra-Physics 125A) was used as the light source. As shown in Fig. 12, the laser beam is divided into two parts—the object beam O and reference beam R. The object beam travels to the twisted plate and then to the photographic plate (Agfa-Gevaert 10E75). The reference beam goes directly to the photographic plate via a mirror. The interference of the two beams at the photographic plate enables a hologram (real-time or time-average) to be made of the twisted plate.

The plates were fabricated from 6061-T4 aluminum sheet stock and had the properties previously ascribed to the finite element model. The axial twist was achieved by placing the plate root in one grip of a machinist's lathe and the plate tip in the other grip. The tip was then manually twisted while the root was held fixed until the desired tip twist was achieved. This method had some obvious disadvantages such as work hardening effects and a small amount of torsional buckling occurring at the larger tip twist angles. It was, however, expedient and the resulting plates served their intended purpose. Six plates were fabricated having tip twist angles (Θ_T) as given in Table 2.

The first ten natural frequencies and mode shapes were experimentally determined for each of the twisted cantilever plates. The frequencies are shown in the "Exp" col-

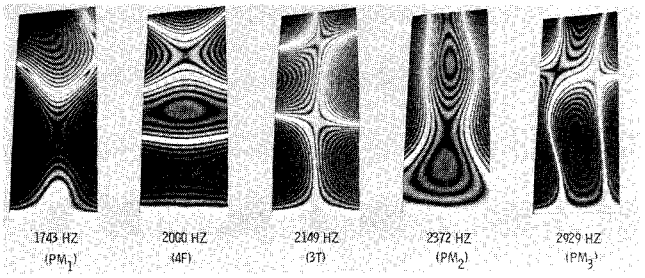

Fig. 14 Experimental mode shapes 6–10 of cantilevered plate ($\Theta_T = -30°$).

umn of Table 2 in terms of the nondimensional frequency, λ. The agreement between the finite element analysis and experimental results is quite good. In general, the agreement between the flexural modes of vibration is better than that between the torsional modes. This is probably due to the fact that the torsional modes are more greatly effected by the plate's axial twist than the flexural modes (see Fig. 4, for example). The axial twist induced in the plates did deviate slightly from the constant linear twist assumed in the finite element models, hence, the greater discrepancy between the finite element and experimental results for the torsional modes.

In addition to determining the natural frequencies, the mode shapes were obtained for the plates. The first ten modes of vibration are shown in Figs. 13 and 14 for the plate having a $-30°$ tip twist. Comparing these results to the finite element results in Figs. 5 and 6, it is seen that the two agree quite well. The advantage of using holographic interferometry to experimentally determine vibration mode shapes is graphically demonstrated by Figs. 13 and 14.

Asymmetry present in some of the modes indicates nonlinear twisting about the plate axis as well as some torsional buckling. As an example of this, note the slight bow in mode $1T$ of Fig. 13 and the asymmetry of modes PM_1 and PM_2 in Fig. 14.

It was not possible to detect the PM_1 mode for either the flat plate ($\Theta_T = 0$) or for the plate with $\Theta_T = -12°$. This not to say that the mode does not exist but only that it is *very* weak when there is little or no axial twist to precipitate the bending-torsional coupling that is characteristic of the mode.

Conclusions

The present study has provided some insight into the stress and vibration behavior of cantilevered plates having varying degrees of tip twist. It was found that while the values of the natural frequency are affected by the amount of twist, the general character of the classical vibration modes is not. In this regard, however, the existence and ease of experimental excitation of the coupled bending-torsion modes (mode PM_1) is strongly dependent on the degree of plate twist. It was also found that the coupled bending-torsion mode shape is more strongly effected by centrifugal loading as evidenced by mode PM_1 transforming to a "$3F$" mode when loaded centrifugally.

Finally, good agreement was demonstrated between the NASTRAN finite element analysis and the experimental work using holographic interferometry. The two methods serve to compliment one another quite well.

References

[1]Rosard, D. D., "Natural Frequencies of Twisted Cantilever Plates," *Journal of Applied Mechanics*, Vol. 20, June 1953, pp. 241–244.

[2]Carnegie, W., "Vibrations of Pre-Twisted Cantilever Blading," *Proceedings of the Institution of Mechanical Engineers*, Vol. 173, 1959, pp. 343–374.

[3]Isakson, G. and Eisely, J. G., "Natural Frequencies in Coupled Bending and Torsion of Twisted Rotating and Non-Rotating Blades," CR-65, July 1964, NASA.

[4]Houbolt, J. C. and Brooks, G. W., "Differential Equations of Motion for Combined Flapwise Bending, Chordwise Bending, and Torsion of Twisted Nonuniform Rotor Blades," Rept. 1346, 1958, NACA.

[5]Anderson, R. G., Irons, B. M., and Zienkiewicz, O. C., "Vibration and Stability of Plates using Finite Elements," *International Journal of Solids and Structures*, Vol. 4, Oct. 1968, pp. 1031–1055.

[6]Rawtani, S. and Dokainish, M. A., "Vibration Analysis of Pretwisted Cantilever Plates," *CASI Transactions*, Vol. 2, Sept. 1969, pp. 95–100.

[7]Dokainish, M. A. and Rawtani, S., "Vibration Analysis of Rotating Cantilever Plates," *International Journal for Numerical Methods in Engineering*, Vol. 3, April, 1971, pp. 233–248.

[8]MacNeal, R. H., ed. *The NASTRAN Theoretical Manual*, SP-221(01), April 1972, NASA.

[9]Barton, M. V., "Vibration of Rectangular and Skew Cantilever Plates," *Journal of Applied Mechanics*, Vol. 18, June 1951, pp. 129–134.

[10]Kelly, B. M., "The NASTRAN Contour Plotter," TM X-2637, Sept. 1972, pp. 385–397, NASA.

[11]Henry, R., "Calcul des coques minces en grande deformations par elements finis application aux aubes de compresseur en rotation," Ph.D. thesis, Structural Mechanics Laboratory, Lyon, France, 1973.

[12]Powell, R. and Stetson, K. A., "Interferometric Vibration Analysis by Wavefront Reconstruction," *Journal of the Optical Society of America*, Vol. 55, Dec. 1965, pp. 1593–1598.

[13]Stetson, K. A. and Powell, R., "Interferometric Hologram Evaluation and Real-Time Vibration Analysis of Diffuse Objects," *Journal of the Optical Society of America*, Vol. 55, Dec. 1965, pp. 1694–1695.

[14]Collier, R. J., Burckhardt, C. B., and Lin, L. H., *Optical Holography*, Academic Press, New York, 1971, pp. 420–453.